AIAA 81-0329R

Alternating-Direction Implicit Algorithm for Unsteady Potential Flow

Richard Chipman*
Grumman Aerospace Corporation, Bethpage, N.Y.
and
Antony Jameson†
Princeton University, Princeton, N.J.

An implicit finite-difference scheme is presented for the efficient computation of unsteady potential flow about airfoils. The formulation uses density and the velocity potential as dependent variables and is cast in conservation form to assure the theoretically correct determination of shockwave location and speed. To enable boundary conditions to be imposed directly on the airfoil surface, a time-varying sheared-rectilinear coordinate transformation is employed. Calculated time-history solutions on a pulsating airfoil are compared with the results of other unsteady transonic codes, including a previous method of the authors. The present method is demonstrated to be unconditionally stable and to give accurate solutions with sharply resolved shocks.

Nomenclature

a	= local speed of sound
$D_x(\ )$	= central difference in x of enclosed quantity
$D_y(\ )$	= central difference in y of enclosed quantity
$\{f(T,\{W\})\}$	= vector function of T and the vector W
h	= stagnation enthalpy
J	= Jacobian of transformation
M	= Mach number
$(\ )^n$	= nth time level of enclosed quantity
$r1,r2$	= right-hand side of Eq. (9) or (26)
$S(x,t)$	= instantaneous airfoil-surface location
t,T	= time
u,U	= streamwise component of velocity, ξ-aligned contravariant velocity component
v,V	= stream-normal component of velocity, η-aligned contravariant velocity component
$\{W\}$	= general vector (in this case, having components ρ and ϕ)
x,y	= untransformed coordinates
$z(x,y,t)$	= surface of flow discontinuity
γ	= specific heat ratio
$\Delta(\ )$	= time increment of enclosed quantity
ϵ	= artificial viscosity coefficient
ξ,η	= transformed coordinates
μ	= see Eq. (6)
ρ	= density
ϕ	= velocity potential
$(\ )_m$	= partial derivative of enclosed quantity with respect to m variable
$(\ )_\infty$	= freestream value of enclosed quantity
$\Delta(\hat{\ })$	= solution to Eq. (11)

Introduction

THE transonic flow regime long has been known to be the most critical for flutter and other unsteady aeroelastic phenomena. Until recently, there was no efficient method for calculating unsteady aerodynamics in this speed range; consequently, transonic flutter prediction has relied on wind-tunnel testing. With the advent of faster computers and the emphasis on transonic cruise and maneuver capabilities for new aircraft design, much progress has been made recently in the development of both steady and unsteady transonic computational methods.

In unsteady transonic aerodynamics, work has proceeded along two distinct lines. In the first, researchers have produced linearized unsteady solutions about nonlinear mean (steady) flows. The efforts of Ehlers,[1] Traci et al.,[2] Cunningham,[3] Liu,[4] and Fung et al.[5] are examples of this approach. From experimental measurements, such as those of Tijdeman,[6] it has been obvious that these linearized solutions are only valid for a limited set of problems. Consequently, other researchers have pursued a second approach—the use of finite-difference methods to obtain solutions to the coupled steady/unsteady flow. In this area, the works of Magnus and Yoshihara,[7] Lerat and Sides,[8] Beam and Warming,[9] Ballhaus and Steger,[10] Ballhaus and Goorjian,[11,12] Isogai,[13] Chipman and Jameson,[14] Goorjian,[15] Sankar and Tassa,[16] and Steger and Caradonna[17] are notable. The first three cited efforts in coupled steady/unsteady flow have produced methods for solving the full Euler equations, which (although computationally too expensive for routine use) do provide excellent benchmark calculations. Ballhaus' works have produced an efficient method for solving the low-frequency, small-perturbation form of the potential equation, thus making possible economic solutions to a range of important transonic unsteady problems.

To extend this range, the latter four works have solved the full-potential flow equations. Isogai developed the first such procedure. The next two works are improvements in that: 1) conservation-law form is used to locate accurately shock waves in space and time; and 2) the ADI scheme is used for computational efficiency. The Chipman-Jameson method uses density and velocity components as dependent variables, giving a simple system of first-order equations to be solved. The Goorjian method uses velocity potential as the dependent variable and, by time linearizing the density, derives a single (though complicated) scalar equation. The method of Sankar and Tassa uses the strongly-implicit-procedure algorithm and has been formulated both in conservative and nonconservative form; thus far, the scheme has been coded only in nonconservative form. The method of Steger and Caradonna is similar to Goorjian's method and, although formulated to include a general time-varying airfoil-adapted grid (such as used by Goorjian and the present authors), the reported applications to date have applied the boundary conditions on the fixed mean plane.

Presented as Paper 81-0329 at the AIAA 19th Aerospace Sciences Meeting, St. Louis, Mo., Jan. 12-15, 1981; submitted March 9, 1981; revision received July 20, 1981.

*Engineering Specialist in Aeroelasticity Methods. Member AIAA.
†Professor, Aeronautical Engineering.

The present method uses both the density and velocity potential as dependent variables, resulting in a simple system of two equations. It is a significant improvement over the authors' previous method[14] in that the use of the potential function totally eliminates numerically created vorticity present in the prior method. Furthermore, it retains the desirable features of conservation form and efficient implicit differencing.

Theory

Basic Flow Equations

For unsteady, two-dimensional, isentropic potential flow, the equations of conservation of mass and momentum can be written

$$\rho_t + (\rho\phi_x)_x + (\rho\phi_y)_y = 0 \tag{1}$$

$$\phi_t + h = 0 \tag{2}$$

where

$$h = \frac{1}{2}(\phi_x^2 + \phi_y^2) + \frac{\rho^{\gamma-1}}{(\gamma-1)M_\infty^2} - h_\infty \tag{3}$$

Both equations are in conservation form, albeit Eq. (2) is considered weak-conservation form. Hence, Eq. (1) conserves mass across shocks, where the flow variables are discontinuous, and results in the jump condition

$$[\rho]z_t + [\rho u]z_x + [\rho v]z_y = 0 \tag{4}$$

where $z(x,y,t) = 0$ represents the surface of discontinuity and [ ] denotes the jump of the enclosed variables across the discontinuity.

Implicit Algorithm

To simplify the ensuing discussion, Eqs. (1) and (2) are represented by the vector equation

$$\{W\}_t + \{f(t,\{W\})\} = 0 \tag{5}$$

A family of difference schemes for solving this system is

$$\{\Delta W\} + \mu\Delta t\{f^{n+1}\} + (1-\mu)\Delta t\{f^n\} = 0 \quad 0 \le \mu \le 1 \tag{6}$$

where n and $n+1$ denote the present and new time levels. For $\mu = 0$, the scheme is explicit; otherwise it is implicit. The case $\mu = \frac{1}{2}$ is the standard Crank-Nicolson scheme,[18] which has second-order accuracy. Using a Taylor series expansion, the variables at the new time can be written

$$\{f^{n+1}\} = \{f^n\} + (\partial/\partial t)\{f^n\}\Delta t + O(\Delta t^2)$$

$$= \{f^n\} + \nabla\cdot\{\Delta W\}\{f^n\} + O(\Delta t^2) \tag{7}$$

Substitution into Eq. (6) gives

$$\{\Delta W\} + \mu\Delta t(\nabla\cdot\{\Delta W\})\{f^n\} = -\Delta t\{f^n\} - O(\Delta t^2) \tag{8}$$

where all coefficients appear at time n.

This scheme is now rewritten in the original variables of Eqs. (1) and (2), and centered differences are used to evaluate the divergence terms. Thus, the following system of equations is obtained for each interior point of the computational grid:

$$\begin{bmatrix} 1+\mu\Delta t(D_x u + D_y v) & \mu\Delta t(D_x\rho D_x + D_y\rho D_y) \\ \mu\Delta t(a^2/\rho) & 1+\mu\Delta t(uD_x + vD_y) \end{bmatrix} \times \begin{Bmatrix} \Delta\rho \\ \Delta\phi \end{Bmatrix} = \begin{Bmatrix} r1 \\ r2 \end{Bmatrix} \tag{9}$$

where

$$\begin{Bmatrix} r1 \\ r2 \end{Bmatrix} = -\Delta t \begin{Bmatrix} D_x\rho u + D_y\rho v \\ h \end{Bmatrix}$$

$$u = \phi_x, \quad v = \phi_y, \quad \Delta(\ ) = (\ )^{n+1} - (\ )^n$$

Approximate Factorization

The matrix on the left-hand side of Eq. (9) can be factored approximately as

$$\begin{bmatrix} 1+\mu\Delta tD_y v & \mu\Delta tD_y\rho D_y \\ \mu\Delta t(a^2/\rho) & 1+\mu\Delta tvD_y \end{bmatrix} \begin{bmatrix} 1+\mu\Delta tD_x u & \mu\Delta tD_x\rho D_x \\ 0 & 1+\mu\Delta tuD_x \end{bmatrix} \tag{10}$$

However, this scheme is not unconditionally stable. A small modification of Eq. (10), which introduces error of order ΔT^3, does result in an unconditionally stable scheme. This modification consists of replacing the lower right-hand term of the second matrix by

$$1 + \mu\Delta tuD_x - \mu^2\Delta t^2(a^2/\rho)D_x\rho D_x$$

The resulting alternating sweeps of this stable scheme are

x-sweep:

$$\begin{bmatrix} 1+\mu\Delta tD_y v & \mu\Delta tD_y\rho D_y \\ \mu\Delta t(a^2/\rho) & 1+\mu\Delta tvD_y \end{bmatrix} \begin{Bmatrix} \Delta\hat{\rho} \\ \Delta\hat{\phi} \end{Bmatrix} = \begin{Bmatrix} r1 \\ r2 \end{Bmatrix} \tag{11}$$

y-sweep:

$$\begin{bmatrix} 1+\mu\Delta tD_x u & \mu\Delta tD_x\rho D_x \\ 0 & 1+\mu\Delta tuD_x - (\mu^2\Delta t^2 a^2/\rho)D_x\rho D_x \end{bmatrix} \times \begin{Bmatrix} \Delta\rho \\ \Delta\phi \end{Bmatrix} = \begin{Bmatrix} \Delta\hat{\rho} \\ \Delta\hat{\phi} \end{Bmatrix} \tag{12}$$

Artificial Viscosity

To capture shocks, artificial-viscosity terms of the Jameson type[19] are added to the upper-left portions of each equation and to $r1$. Respectively, these terms are

$$-\epsilon\Delta t\Delta yD_y^2 \quad -\epsilon\Delta t\Delta xD_x^2 \quad \epsilon\Delta t(\Delta xD_x^2\rho + \Delta yD_y^2\rho) \tag{13}$$

where ϵ is a constant, typically equal to 0.15.

Alternate schemes for incorporating artificial viscosity in a more selective manner are possible. One such alternative is to switch the cofficient from a low value in regions where the flow is subsonic to a higher value in supersonic regions; i.e.,

$$\epsilon = \epsilon_0 + \epsilon_1 \max\left(0, 1 - \left(\frac{M_c}{M}\right)^2\right) \tag{14}$$

where

ϵ_0 = artificial viscosity in "subsonic" zones ($M \le M_c$)
ϵ_1 = maximum amount of artifical viscosity added to "supersonic" zones ($M > M_c$)
M = local Mach number
M_c = cutoff Mach number (typically 0.95)

Another scheme is to vary the viscosity based on gradients in the flowfield; e.g.,

$$\epsilon = \epsilon_0 + \epsilon_1 \left(\frac{\phi_{i+1,j} - 2\phi_{i,j} + \phi_{i-1,j}}{|\phi_{i+1,j}| + 2|\phi_{i,j}| + |\phi_{i-1,j}|}\right) \tag{15}$$

When such schemes are used, however, care must be taken to retain conservation form in the basic equations. Thus, for

example, the first term of Eqs. (13) must be replaced by

$$-\Delta t \Delta y \mathrm{D}_y(\epsilon \mathrm{D}_y) \tag{16}$$

In the present work, only the constant (nonswitched) form of artificial viscosity has been used. Future efforts could easily include the switching concept.

Airfoil-Adapted Coordinate Transformation

To conveniently impose the airfoil boundary conditions, a time-varying coordinate transformation can be introduced to Eqs. (1) and (2). The general form of such a transformation is

$$\xi=\xi(x,y,t), \quad \eta=\eta(x,y,t), \quad T=t \tag{17}$$

Equations (1) and (2) transform as

$$\rho_T+\left(\frac{\rho U}{|J|}\right)_\xi+\left(\frac{\rho V}{|J|}\right)_\eta=0, \quad \phi_T+h=0 \tag{18}$$

where J is the Jacobian of the transformation and U and V are the contravariant velocity components, given by

$$U=\xi_t+\xi_x u+\xi_y v, \qquad V=\eta_t+\eta_x u+\eta_y v \tag{19}$$

To preserve a factorable form of the equations, cross terms arising when Eq. (19) is introduced into Eq. (18) are explicitly differenced. This technique is illustrated subsequently.

For the particular sample problem used in this study, a simple time-varying sheared-rectilinear coordinate transformation is used

$$\xi=x, \quad \eta=y-S(x,t), \quad T=t \tag{20}$$

where S is the instantaneous airfoil surface location as noted in Fig. 1. For this case, the determinant of J is 1 and Eq. (19) becomes

$$U=\phi_\xi-S_\xi\phi_\eta, \qquad V=-\phi_\xi S_\xi+\phi_\eta(1+S_\xi^2)-S_T \tag{21}$$

Substitution into Eq. (18) gives

$$\rho_T+(\rho\phi_\xi)_\xi+(\rho[-S_T+(1+S_\xi^2)\phi_\eta])_\eta=(\rho S_\xi\phi_\eta)_\xi+(\rho S_\xi\phi_\xi)_\eta$$

$$\phi_T+\frac{\rho^{\gamma-1}}{(\gamma-1)M_\infty^2}+\frac{1}{2}[\phi_\xi^2+(1+S_\xi^2)\phi_\eta^2]-h_\infty=S_\xi\phi_\xi\phi_\eta \tag{22}$$

The implicit algorithm developed previously is now applied to this system; however, the cross terms, grouped on the right-hand side of Eq. (22), are handled explicitly. The resulting equations are

$$\Delta\rho+\mu\Delta T\left(\frac{\partial}{\partial\xi}\bar{u}+\frac{\partial}{\partial\eta}[-S_T+\bar{v}]\right)\Delta\rho+\mu\Delta T\left(\frac{\partial}{\partial\xi}\rho\frac{\partial}{\partial\xi}+\frac{\partial}{\partial\eta}\bar{\rho}\frac{\partial}{\partial\eta}\right)\Delta\phi+\Delta T\left(\frac{\partial}{\partial\xi}\rho U+\frac{\partial}{\partial\eta}\rho V\right)=0$$

$$\Delta\phi+\mu\Delta T\left(\frac{a^2}{\rho}\right)\Delta\rho+\mu\Delta T\left(\bar{u}\frac{\partial}{\partial\xi}+\bar{v}\frac{\partial}{\partial\eta}\right)\bar{\Delta}\phi+\Delta T h=0 \tag{23}$$

where a is the local speed of sound and

$$\bar{u}=\phi_\xi, \quad \bar{v}=(1+S_\xi^2)\phi_\eta, \quad \bar{\rho}=(1+S_\xi^2)\rho \tag{24}$$

Replacing the indicated partial derivatives by central-difference operators, D, one obtains the following matrix equation:

$$\begin{bmatrix} 1+\mu\Delta T(\mathrm{D}_\xi\bar{u}+\mathrm{D}_\eta(\bar{v}-S_T)) & \mu\Delta T(\mathrm{D}_\xi\rho\mathrm{D}_\xi+\mathrm{D}_\eta\bar{\rho}\mathrm{D}_\eta) \\ \mu\Delta T(a^2/\rho) & 1+\mu\Delta T(\bar{u}\mathrm{D}_\xi+\bar{v}\mathrm{D}_\eta) \end{bmatrix} \times \begin{Bmatrix} \Delta\rho \\ \Delta\phi \end{Bmatrix} = -\Delta T \begin{Bmatrix} \mathrm{D}_\xi\rho U+\mathrm{D}_\eta\rho V \\ h \end{Bmatrix} \tag{25}$$

Following the factorization procedure previously outlined and introducing the artificial viscosity terms, one obtains the final difference equations

ξ-sweep:

$$\begin{bmatrix} 1+\mu\Delta T\mathrm{D}_\eta(\bar{v}-S_T)-\epsilon\Delta T\Delta\eta\mathrm{D}_\eta^2 & \mu\Delta T\mathrm{D}_\eta\bar{\rho}\mathrm{D}_\eta \\ \mu\Delta T(a^2/\rho) & 1+\mu\Delta T\bar{v}\mathrm{D}_\eta \end{bmatrix} \begin{Bmatrix} \Delta\hat{\rho} \\ \Delta\hat{\phi} \end{Bmatrix} = -\Delta T \begin{Bmatrix} r1 \\ r2 \end{Bmatrix} \tag{26}$$

where

$$\begin{Bmatrix} r1 \\ r2 \end{Bmatrix} = \begin{Bmatrix} \mathrm{D}_\xi\rho U+\mathrm{D}_\eta\rho V-\epsilon(\Delta\xi\mathrm{D}_\xi^2+\Delta\eta\mathrm{D}_\eta^2)\rho \\ h \end{Bmatrix}$$

η-sweep:

$$\begin{bmatrix} 1+\mu\Delta T\mathrm{D}_\xi\bar{u}-\epsilon\Delta T\Delta\xi\mathrm{D}_\xi^2 & \mu\Delta T\mathrm{D}_\xi\rho\mathrm{D}_\xi \\ 0 & 1+\mu\Delta T\bar{u}\mathrm{D}_\xi-(\mu^2\Delta T^2a^2/\rho)\mathrm{D}_\xi\rho\mathrm{D}_\xi \end{bmatrix} \times \begin{Bmatrix} \Delta\rho \\ \Delta\phi \end{Bmatrix} = \begin{Bmatrix} \Delta\hat{\rho} \\ \Delta\hat{\phi} \end{Bmatrix} \tag{27}$$

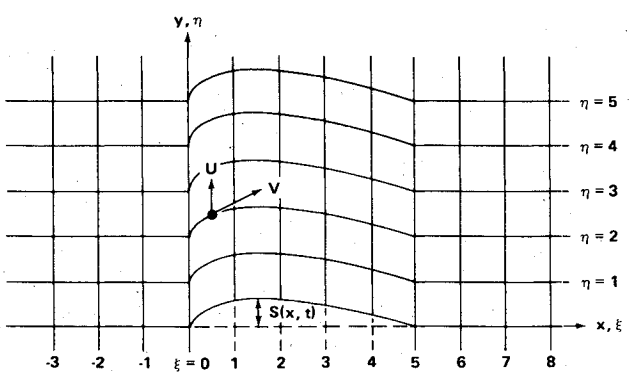

Fig. 1 Shearing transformation.

Discretization

In Eqs. (26) and (27), differences will be centered about (i,j) and will span two mesh widths (three points); consequently, the operators $(\mathrm{D}_\eta\rho\mathrm{D}_\eta)$ and $(\mathrm{D}_\xi\rho\mathrm{D}_\xi)$ will spread to four mesh widths (five points). The equation for the jth mesh point in Eq. (26) may then be written in the form

$$[A]\{\Delta\hat{W}\}_{j-2}+[B]\{\Delta\hat{W}\}_{j-1}+[C]\{\Delta\hat{W}\}_j+[D]\{\Delta\hat{W}\}_{j+1}+[E]\{\Delta\hat{W}\}_{j+2}=\{r\} \tag{28}$$

where the coefficients of $\{\Delta W\}$ for mesh points outside the range $j-2$ to $j+2$ are zero. If Eq. (26) is multiplied by

$2(\Delta\eta)_j/\Delta T$, the coefficients in Eq. (28) become

$$[A]=\begin{bmatrix} 0 & (\bar{\rho}/2\Delta\eta)_{j-1} \\ 0 & 0 \end{bmatrix},\quad [E]=\begin{bmatrix} 0 & (\bar{\rho}/2\Delta\eta)_{j+1} \\ 0 & 0 \end{bmatrix}$$

$$[B]=\begin{bmatrix} (\bar{v}-S_T)_{j-1} & 0 \\ 0 & \bar{v}_j \end{bmatrix},\quad [D]=\begin{bmatrix} (-\bar{v}+S_T)_{j+1} & 0 \\ 0 & -\bar{v}_j \end{bmatrix}$$

$$[C]=\begin{bmatrix} (2/\mu\Delta t)\Delta\eta_j+(4\epsilon/\mu) & -(\bar{\rho}/2\Delta\eta)_{j-1}-(\bar{\rho}/2\Delta\eta)_{j+1} \\ 2(\Delta\eta a^2/\rho)_j & (2/\mu\Delta T)\Delta\eta_j \end{bmatrix} \tag{29}$$

A similar set of matrices can be obtained from Eq. (27).

Stretchings

For computational efficiency, simple grid stretchings also are introduced

$$\bar{\xi}=\bar{\xi}(\xi) \quad \text{and} \quad \bar{\eta}=\bar{\eta}(\eta) \tag{30}$$

The effect of these transformations on the equations to be solved is simply to introduce the derivatives of the stretching functions as multipliers of the terms containing spatial derivatives. The details of the particular stretchings used are discussed in the Sample Problem subsection.

Solution Procedure

If equations similar to Eq. (28) are written for all mesh points and combined into one system corresponding to Eq. (26), the result is a system of block-five-diagonal matrix equations. This can be solved efficiently by an LU decomposition. Thus, Eq. (26) is rewritten as

$$[L][U]\{\Delta\hat{W}\}=\{r\} \tag{31}$$

and the solution is obtained by sequentially solving

$$[L]\{b\}=\{r\} \qquad [U]\{\Delta\hat{W}\}=\{b\} \tag{32}$$

where $[L]$ and $[U]$ are lower and upper tridiagonal matrices, respectively. An identical procedure is used to obtain a solution for Eq. (27).

To initialize and terminate the sweeps, the difference equations are modified to incorporate the presence of the boundaries. At the lower boundary, for example, we choose to backward difference the ρ- and v-type terms (so that no physical variables are defined outside the computational space) and to retain central differences in ϕ terms by introducing a row of dummy points just below $\eta=0$. Before and after the sweeps are completed, the boundary conditions (discussed next) are enforced.

Boundary Conditions

On the airfoil surface, tangential flow is maintained. In the transformed coordinates, this is equivalent to

$$V=0, \quad \text{for } \eta=0 \text{ and } \xi_{LE}\le\xi\le\xi_{TE} \tag{33}$$

where subscripts LE and TE denote the airfoil leading and trailing edges, respectively. For the nonlifting symmetric-airfoil problem studied, the flow is symmetric about $\eta=0$; consequently, only half the flowfield is modeled. Thus,

$$\phi_\eta=0, \quad \text{for } \eta=0 \text{ and } \xi\le\xi_{LE} \text{ or } \xi\ge\xi_{TE} \tag{34}$$

The uniform onset flow in the far field is assumed to be undisturbed; i.e., acoustic waves originating at the airfoil do not have sufficient time to reach the outer boundaries. Thus,

$$(u,v)=(1,0)$$

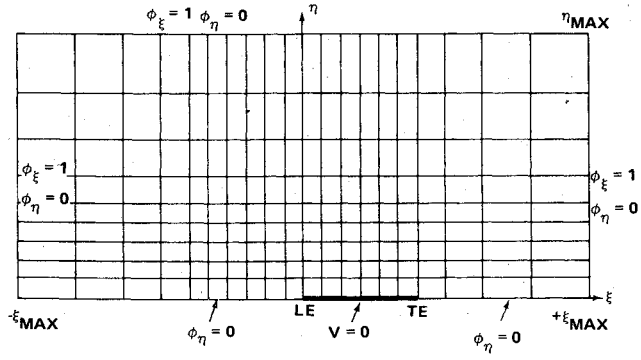

Fig. 2 Boundary conditions in the computational grid.

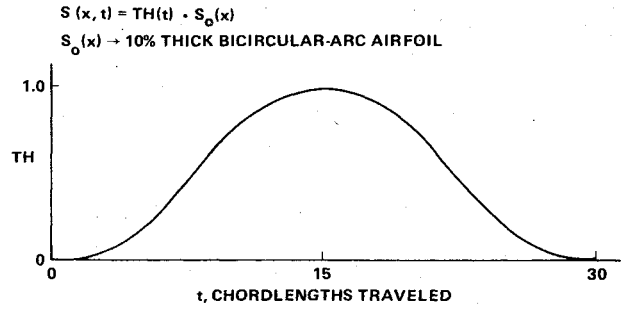

Fig. 3 Pulsating parabolic-arc airfoil.

or

$$v=\phi_\eta=0, \quad u=\phi_\xi-S_\xi\phi_\eta=\phi_\xi=1$$

Hence,

$$(\phi_\xi,\phi_\eta)=(1,0), \quad \text{for } \eta=\eta_{max} \text{ and } \xi=\pm\xi_{max} \tag{35}$$

where the subscripts max denote the far-field boundaries of the computational mesh. In Fig. 2, the boundary conditions are marked on a sketch of the computational space.

Implementation (Codes UFLO3 and UFLO4)

The algorithm was coded for the pulsating-airfoil sample problem to be described next. A version (UFLO3) using the original untransformed equations was written, as well as a version (UFLO4) employing the time-varying coordinates. For UFLO3, the airfoil boundary conditions were applied on the slit, $y=0$ (mean chordline); whereas, in UFLO4, they were applied on the $\eta=0$ line coincident with the instantaneous airfoil surface position.

Results

Sample Problem

A problem that has been analyzed by several researchers is that of computing unsteady pressures on a parabolic-arc airfoil which successively thickens and thins during its travel, as shown in Fig. 3. The Mach number for this example is 0.85. The equations governing the variation of thickness are

$$TH=\frac{1}{10}\left[10-15\left(\frac{T}{15}\right)+6\left(\frac{T}{15}\right)^2\right]\left(\frac{T}{15}\right)^3, \quad 0\le T\le 15$$

$$TH=\frac{1}{10}\left[10-15\left(\frac{30-T}{15}\right)+6\left(\frac{30-T}{15}\right)^2\right]\left(\frac{30-T}{15}\right)^3,$$

$$15\le T\le 30$$

$$TH=0, \quad 30\le T \tag{36}$$

where TH is the midchord thickness ratio and T is the time, measured in chordlengths traveled. Consequently, the airfoil initially has zero thickness, grows to its maximum thickness of 10% after traveling 15 chordlengths and returns to zero thickness after traveling a total of 30 chordlengths. During the course of this travel, the variation of thickness causes an interesting flow structure. A strong shock wave forms on the airfoil as it thickens; subsequently, as the airfoil thins, the shock propagates rapidly upstream and leaves the airfoil nose to enter the oncoming flow. The numerical computation of this extensive shock motion is a rigorous test for unsteady transonic aerodynamic codes. It might be noted that, because of their basic theoretical limitations, the methods of Refs. 1-5 are unable to handle such cases of large shock motion.

The computational grid used consists of 152 points in the streamwise direction and 40 in the stream-normal direction. To facilitate comparisons, the grid is patterned after that of Ref. 15. In the streamwise direction, the grid is uniform over the interval that extends from one chordlength upstream of the airfoil nose to the trailing edge; to either side of this interval, the grid is smoothly stretched to the boundaries located more than 30 chordlengths from the airfoil. In the stream-normal direction, the grid is uniform from the airfoil surface to a distance of 0.2 chordlengths; beyond this point, the grid is stretched smoothly to a boundary also more than 30 chordlengths from the airfoil. The minimum grid spacing is roughly 0.02 chordlengths in each direction. From studies of grid variation, it was concluded that the solution is sensitive to the choice of grids but that the present choice is adequate because it combines a fine-grid structure near the airfoil with boundaries sufficiently far removed for the present calculations.

Unless otherwise noted, all calculations using either UFLO3 or UFLO4 were performed with a time step of $\Delta T = 0.02$ chordlengths traveled and an artificial viscosity coefficient of $\xi = 0.15$.

UFLO3 and UFLO4 Results

Using UFLO3, a time history of the flow about the pulsating airfoil was calculated. The resulting pressure coefficient distributions for six time slices are shown in Fig. 4. At the first time slice, the flow is subcritical. During the next two, a shock forms, strengthens, and moves aft. A slight re-expansion occurring behind the shock can be seen in Fig. 4a. It should be noted that a significant lag occurs between the time that the airfoil reaches maximum thickness ($T = 15$) and the point at which maximum shock strength is attained ($T = 18.25$). In the next three time slices (note that different scales are used), the shock moves rapidly forward, while diminishing in strength, and leaves the airfoil.

To determine the effect of applying the boundary conditions on the slit rather than the actual airfoil surface, results of UFLO3 and UFLO4 are compared in Fig. 5. To obtain a more dramatic difference, a 15% airfoil was used in place of the 10% airfoil previously studied; consequently, different time slices are shown. At the early time slices (Fig. 5a), during which the shock is formed, the results are practically identical. At later times noticeable differences occur. Comparing time $T = 15$ (Fig. 5b) with $T = 25$ (Fig. 5c) and time $T = 25$ with $T = 30$ (Fig. 5c), one sees that the shock speeds computed by UFLO3 during these time intervals are greater than those computed by UFLO4 (in which the boundary conditions are correctly applied on the airfoil surface). A comparison of time $T = 30$ with $T = 35$ indicates that this trend persists even after the airfoil has returned to zero thickness.

Comparison with Other Methods

Two other codes (Refs. 14 and 15) exist that solve the unsteady-potential-flow equations in conservation form on a time-varying airfoil-adapted grid. To compare these methods with the present code, results for the pulsating-airfoil problem are presented in Fig. 6. In this instance, the time history of the

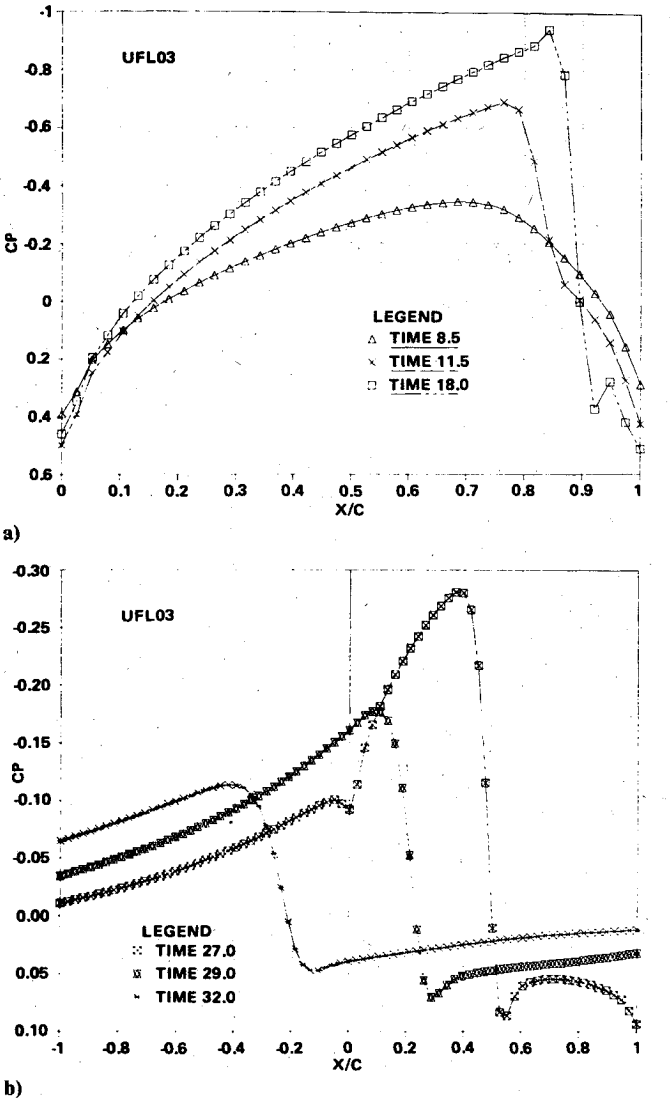

Fig. 4 Time history of pressure on pulsating airfoil computed by UFLO3; a) during shock buildup and b) during shock propagation.

midchord pressure coefficient is plotted. As can be seen, all three methods give practically the same results up to the time at which the shock passes; thereafter, the results of Ref. 14 differ from those of Ref. 15 and the present method. Reference 14 is an earlier formulation of the present authors, which uses primitive variables (ρ, u, v) rather than the potential function itself. It is believed that erroneous vorticity is created numerically by the method—particularly behind strong shocks—and that this mechanism is responsible for degrading the solution. (This shortcoming was part of the motivation for developing the present method.)

Also shown in Fig. 6 are the results of Ref. 10, a low-frequency, small-perturbation solution. The principal difference between these results and those of the full-potential methods is a more rapid pressure buildup that results in the maximum midchord pressure occurring roughly two chordlengths traveled earlier in time.

From the previous comparisons, it is apparent that the present method and that of Ref. 15 are in good agreement. To further expand this point, Fig. 7 is presented comparing the pressure coefficient distributions at two time slices, $\tau = 18$ and 32. At the earlier time (Fig. 7a), UFLO4 is seen to predict a slightly farther aft shock; but, since the shock-location difference is only one mesh width, this discrepancy is considered insignificant. Figure 7b shows that, during shock propagation, the shock computed in Ref. 15 is smeared over a larger distance and has attenuated more than that of UFLO4.

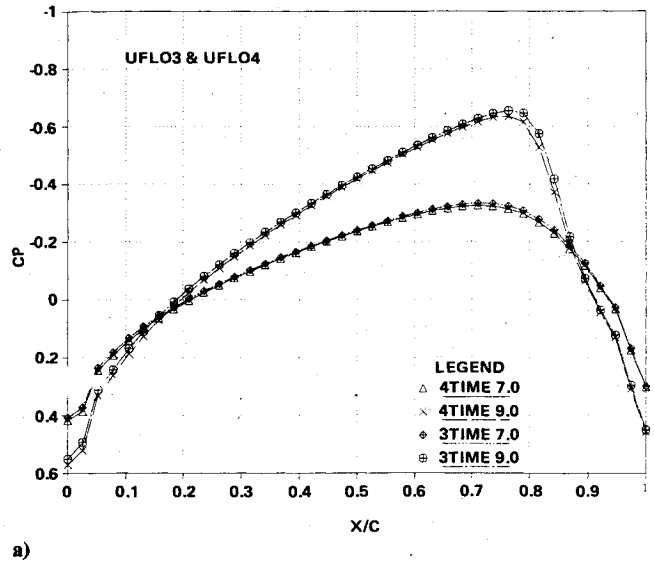

a)

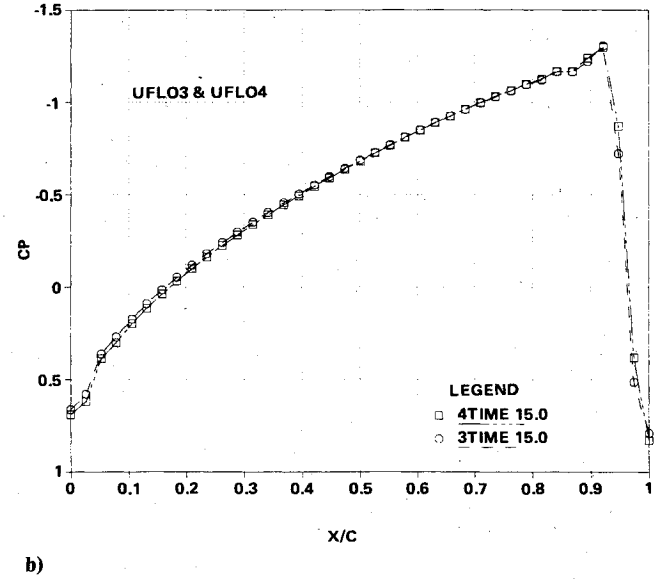

b)

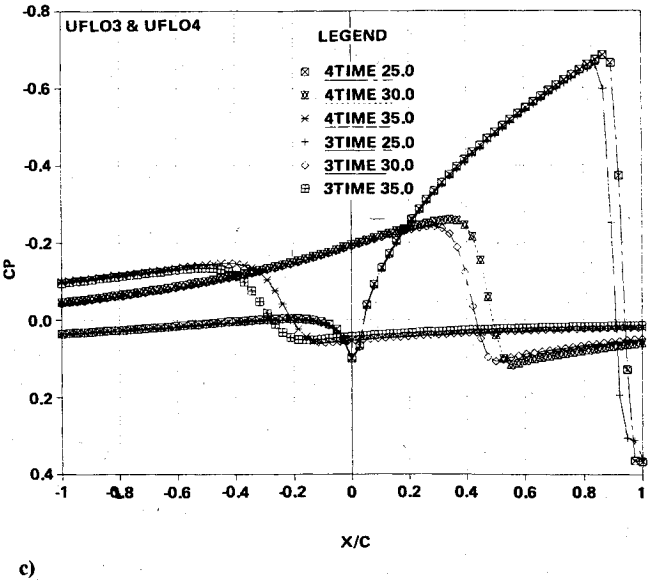

c)

Fig. 5 Comparison of UFLO3 and UFLO4 for a 15%-thick airfoil; a) $T = 7$ and 9, b) $T = 15$, and c) $T = 25$ and 30.

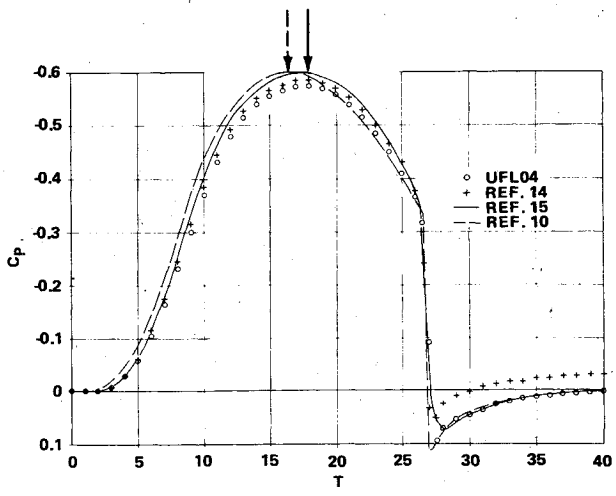

Fig. 6 Time history of midchord pressure coefficient.

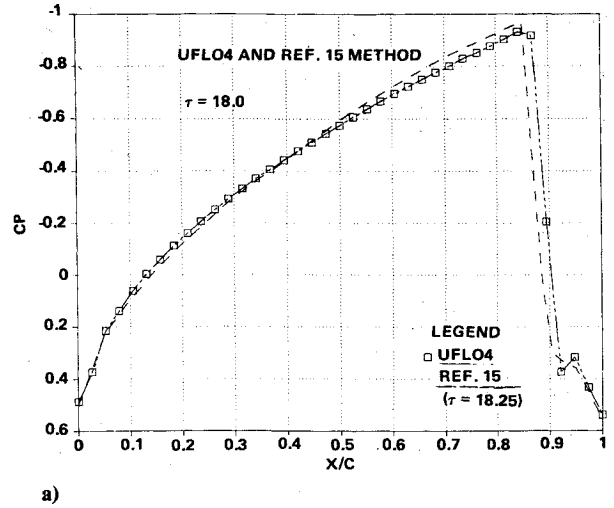

a)

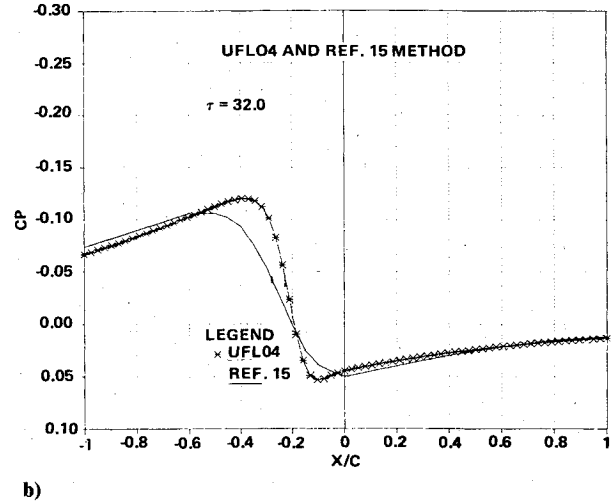

b)

Fig. 7 Comparison of UFLO4 with Ref. 15; a) $T \simeq 18$ and b) $T = 32$.

The better shock resolution of the present method is considered to be due to the use of a five-point difference scheme and artificial viscosity in lieu of the three-point scheme and artificial compressibility used in Ref. 15. In summary, the comparisons show that the present method and that of Ref. 15 give almost equivalent results for the sample problem. The only significant difference in the solutions is the degree of shock smearing and, in this aspect, the present program appears to perform somewhat better.

Stability, Accuracy, and Computing Time

Various runs of both UFLO3 and UFLO4 were made to determine the effect of the time step on stability and accuracy. For the sample problem, the computations were numerically stable for the largest time step ($\Delta T = 0.2$) run; however, accuracy degenerated above the step of $\Delta T = 0.033$. Since, for nonzero mesh widths, the artificial viscosity terms in Eqs. (26) and (27) can be thought of as error terms of order ΔT, any reduction in these terms should improve accuracy for a given step size. Thus, it is likely that, by reducing the amount of artificial viscosity, accurate solutions could be obtained with a somewhat larger step size than the 0.033 discussed earlier.

The computational time required for the algorithm is roughly 7.0×10^{-5} s per time step per grid point on the CDC 7600 computer. For the sample problem with $\Delta T = 0.033$, the time required for a time history of 32 chordlengths traveled is about 6 min.

Concluding Remarks

An accurate algorithm with excellent numerical stability has been developed for the two-dimensional unsteady full-potential equation in conservation form, using time-varying sheared-rectilinear, body-conforming coordinates. The method has been demonstrated on the highly nonlinear transonic flow arising from an airfoil with pulsating thickness. The results of this demonstration have been verified by comparison with those reported in various references.

Two recommendations are made to increase the accuracy and efficiency of the procedure. The first is to introduce switched artificial viscosity as discussed in the Theory section. This change would localize the artificial-viscosity terms to regions where they are needed, thereby improving the accuracy for a given time step. Consequently, larger time steps could be used with a resultant decrease in computing time. The second suggestion is to modify the manner in which the operators $D_\xi \rho D_\xi$ and $D_\eta \bar{\rho} D_\eta$ in Eqs. (26) and (27) are evaluated. A three-point scheme could be constructed in place of a five-point scheme. To accomplish this, densities midway between mesh points would be evaluated by averaging the values from the two adjacent nodes. This modification would result in reducing the system in Eq. (31) from block-five diagonal to block-three diagonal. It can be shown that the computing time required to solve the smaller bandwidth system is roughly half that required for the larger system.

To enable the method to handle realistic blunt-nosed airfoils, it is planned to modify the code to use a curvilinear coordinate transformation. Additionally, extensions to the case of a lifting airfoil and improved treatment of the far-field boundary conditions will be undertaken.

Acknowledgments

The authors wish to thank E. J. Laurie of Grumman Aerospace for assistance in running the comparison calculations presented in this paper and in generating the computer-graphics displays. The work was supported by NASA Ames Contract NAS 2-10487. Funding was provided jointly by the Applied Computational Aerodynamics Branch of NASA Ames and the Structural Mechanics Division of AFWAL.

References

[1] Ehlers, F. E., "A Finite Difference Method for the Solution of the Transonic Flow Around Harmonically Oscillating Wings," NASA CR-2257, July 1974.

[2] Traci, R. M., Albano, E. D., and Farr, J. L., "Perturbation Method for Transonic Flows About Oscillating Airfoils," *AIAA Journal*, Vol. 14, Sept. 1976, pp.

[3] Cunningham, A. M., "An Oscillatory Kernel Function Method for Lifting Surfaces in Mixed Transonic Flow," AIAA Paper 74-359, April 1974.

[4] Liu, D. D., "A Lifting Surface Theory Based on an Unsteady Linearized Transonic Flow Model," AIAA Paper 78-501, April 1978.

[5] Fung, F. Y., Yu, N. J., and Seebass, R., "Small Unsteady Perturbations in Transonic Flows," *AIAA Journal*, Vol. 16, Aug. 1978, pp. 815-822.

[6] Tijdeman, H., "Investigation of the Transonic Flow Around Oscillating Airfoils," NLR Rept. TR 77090 U, 21-X-1977.

[7] Magnus, R. J. and Yoshihara, H., "Unsteady Transonic Flow Over an Airfoil," *AIAA Journal*, Vol. 14, Dec. 1975, pp. 1622-1628.

[8] Lerat, A. and Sides, J., "Calcul Numerique D'ecoulements Transsoniques Instationnaires," ONERA TP No. 1977-19E, April 1977.

[9] Beam, R. M. and Warming, R. F., "Numerical Calculations of Two-Dimensional Unsteady Transonic Flows with Circulation," NASA TN D-7605, Feb. 1974.

[10] Ballhaus, W. F. and Steger, J. L., "Implicit Approximate-Factorization Schemes for the Low-Frequency Transonic Equation," NASA TM X-73,082, Nov. 1975.

[11] Ballhaus, W. F. and Goorjian, P. M., "Implicit Finite Difference Computations of Unsteady Transonic Flows about Airfoils," *AIAA Journal*, Vol. 15, Dec. 1977, pp. 1728-1735.

[12] Ballhaus, W. F., and Goorjian, P. M., "Computation of Unsteady Transonic Flows by the Indicial Methods," *AIAA Journal*, Vol. 16, Feb. 1978, pp. 117-124.

[13] Isogai, K., "Calculation of Unsteady Transonic Flow Over Oscillating Airfoils Using the Full Potential Equation," AIAA Paper 77-448, April 1977.

[14] Chipman, R. and Jameson, A., "Fully Conservative Numerical Solutions for Unsteady Irrotational Transonic Flow about Airfoils," AIAA Paper 79-1555, July 1979.

[15] Goorjian, P. M., "Computations of Unsteady Transonic Flow Governed by the Conservative Full Potential Equation Using an Alternating Direction Implicit Algorithm," NASA CR-152274, June 1979, and AIAA Paper 80-0150, Jan. 1980.

[16] Sankar, N. L. and Tassa, Y., "An Algorithm for Unsteady Transonic Potential Flow Past Airfoils," paper presented at the Seventh International Conference on Numerical Methods in Fluid Dynamics, June 1980.

[17] Steger, J. and Caradonna, F., "A Conservative Implicit Finite Difference Algorithm for the Unsteady Transonic Full Potential Equation," AIAA Paper 80-1368, July 1980.

[18] Isaacson, E. and Keller, H. B., *Analysis of Numerical Methods*, Wiley and Sons, Inc., New York, 1966.

[19] Jameson, A., "Transonic Flow Calculations," Notes of Lecture presented at the Von Karman Institute, Belgium, March 1976.